# EFFECT OF LOCAL BUCKLING AND WORK-HARDENING PROPERTIES OF STEEL MATERIAL ON THE BEHAVIOR OF I-BEAM SUBJECTED TO LATERAL CYCLIC LOAD

Raafat El-Sayed SHAKER*, Hidekazu MURAKAWA** and Yukio UEDA***

The hysteretic behavior of cantilever I-beam subjected to cyclic lateral loads is investigated in this paper. Finite Element Method (FEM) considering the geometrical and material non-linearities is utilized in this study. Special attention is paid to the effects of local buckling occurring in the flanges and the web, and the material work-hardening properties on the performance of I-beam in view of a seismic design considerations. The behavior of I-beam subjected to cyclic lateral loads is closely examined with respect to the ductility, strength and absorbed energy. From this study, it is found that smaller slenderness ratios of the flange and web are recommended for improving the ductility, strength and absorbed energy. Also, the material having lower yield-to-tensile strength improves the ductility of I-beam under cyclic lateral loads as well as monotonically increasing load.

## 1. Introduction

In the design of seismic resisting frames, it is generally acceptable to allow the frame elements as well as the joint panels to deform plastically beyond its elastic limit. Allowing this plastic deformation enables the structure to dissipate the input earthquake energy. For these reasons, members and joints must be designed and detailed to be capable of deforming well into the inelastic range without causing overall frame instability.

For moment resisting frames subjected to seismic loading, plastic deformation can take place in the girders, columns and panel joints. If the columns and panel joints are designed to be stronger than the girders, then the plastic deformation will concentrate primarily in the girder. This design philosophy is termed " strong column-weak beam design". The aim is to prevent the formation of plastic hinges in the columns that may lead to general frame instability. One of the main problems in the strong column-weak beam design is the development of inelastic local buckling in component plates of the beam which may cause deterioration in the strength and deformation capability of the beam. Well designed section geometry can be considered as a possible solution to improve the performance of the beam against earthquake loading. Another possibility to improve the performance of steel beam is to use materials that achieve high ductility. Therefore, the study of the interaction between the cyclic local buckling and the work-hardening properties of steel material is one of the fundamental research in view of a seismic design consideration [1].

In this paper, the effect of local buckling and work-hardening properties of the material on the behavior of I-beam under both the application of cyclic loading as well as monotonically increasing load is investigated. The Finite Element Method considering material and geometrical non-linearities is employed in this study. At first, the validity of Finite Element

* Graduate Student, Welding Research Institute, Osaka Univ., 11-1, Mihogaoka, Ibaraki, Osaka 567, Japan
** Ph.D., Assoc. Prof., Welding Research Institute, Osaka Univ., 11-1, Mihogaoka, Ibaraki, Osaka 567, Japan
*** Dr., Professor, Welding Research Institute, Osaka University, 11-1, Mihogaoka, Ibaraki, Osaka 567, Japan

modeling to the elasto-plastic large deformation analysis of I-section cantilever beam is examined through two comparisons with an available reported experimental data. Since the phenomena may change with the geometrical parameters of the member and the type of loading, also, may be influenced by material properties, the effect of the following factors are investigated.

1) Geometrical parameters represented by slenderness ratios of the flanges and web
2) Monotonically increasing load and cyclic loading with increasing displacement amplitude
3) Work-hardening properties represented by yield-to-tensile strength ratio

Based on the computed results, the phenomena is examined with respect to the strength, the deformation capability, the stiffness, the energy absorbing capability, the local buckling and the accumulation of local plastic strain. Further, the effect of investigated factors and their interaction are discussed and general conclusions are drawn.

## 2. Computational Method

### 2.1 Elasto-plastic large deformation analysis

The behavior of built-up I-section thin-walled beam is highly non-linear to be analyzed with simple numerical or analytical methods. The difficulty involved in the problem comes from the coexistence of geometrical and material non-linearities due to the elasto-plastic local buckling of the flange and/or the web plates. The Finite Element Method is considered as a very powerful tool for analyzing the inelastic nonlinear behaviors of structural members, and it has wide applicability in various engineering analyses. During the last two decades, the time consumption in non-linear computations by this method put a practical limit on the size of the problems to be handled specially under long history of loading such as cyclic loading. However, due to the progress in computer technology, such non-linear computations can now be conducted with acceptable time consumption on a work station rather on a main frame, from the computational point of view. In this study, the Finite Element Method considering both geometrical and material nonlinearities has been utilized. All computations involved in the present research were performed with a double precision on a YHP-9000/735 work station.

### 2.2 Main features of FEM

For the computation of both the in-plane and the out-of-plane displacements, a flat shell element can be used to model the built-up I-section beam. A simple four node quadrilateral isoparametric flat shell element is used in this study. The main features of this element and the non-linear FEM are summarized as follows.

1) The formulation of this element is based on the assumed displacement field approach.
2) The bending and the in-plane stiffness including their interaction are computed based on the virtual work theorem in incremental form. The bending stiffness matrix is formulated based on the well-known Mindlin plate theory, in which the transverse shear deformations are included [2]. Bilinear shape function is assumed to define the geometry and the displacement fields within the element. A selective reduced integration scheme is adopted to prevent the transverse shear locking [3]. This locking is usually developed when the low order shape function is assumed to define the displacement fields [4] The membrane and bending energy terms are integrated using two-by-two Gaussian quadrature. While the transverse shear energy term is integrated using one-point Gaussian quadrature.
3) For the solution, Total Lagrangian formulation which uses the Green strain tensor and the Second-Piola Kirchoff Stress tensor is employed to describe the kinematic behavior of the element (large deformation).

4) A small strain and plane stress state are assumed in the formulation of constitutive relation.

5) The material plasticity model by Petersson and Popov [5] is adopted in this study. This model is based on the Mroz' multi surface plasticity model with multilinear uniaxial stress-strain relationship, Von Mises yield criterion, and non-linear combined isotoropic-kinematic hardening rule. In this model, the actual material properties are determined from the virgin state (under monotonically increasing load) and saturated state (when steady state of the material are fully developed under cyclic loading) of the material. The transition between these states of the material is controlled by a weighting function $W$ which is a function of the accumulated equivalent plastic strain. The weighting function $W$ can be found by a trial-and-error procedure, as described by Popov and Petersson [5),6]. This model was further developed by Mosaddad and Powel [7], from the computational efficiency point of view. The full kinematic hardening rule can be employed optionally. The layered model with six Gaussian points through the thickness of the element (a total of 24 integration points per element) is used to check the spread of plasticity.

6) An incremental predictor with Newton-Raphson iterations is adopted with the aid of displacement control to trace the complete equilibrium path. Also, the arc-length method [8] is adopted and can be employed optionally. The automatic sizing of load increment based on the current stiffness parameter is also adopted [9]. Convergence of nonlinear solution is controlled by the Euclidian norm of the unbalanced forces.

### 2.3 Validation of Finite Element Modeling

To prove the validity of the modeling to the elasto-plastic large deformation analysis of I-beam , two comparisons were made on built-up I-section cantilever beam subjected to monotonically increasing lateral loads. **Table 1** gives the details of the models used in the comparison with experimental ones reported by [10]. In the analysis, the residual stresses were considered and the idealized pattern is shown in Fig. 1. Since no information regarding the initial imperfection due to fabrication process was reported in the reference, an initial deflection in the form of four sine-waves along the longitudinal direction with the magnitude of .05 times the thickness of each component plates is assumed. Figure 2 shows schematically the assumed initial deflection pattern. This pattern is chosen to include both the flanges and the web buckling modes and to initiate the buckling in the non-linear analysis. In the simulation, the load was applied vertically at point A located at the mid height of the web and 1150 mm from the fixed end. This point was constrained in y-direction which is normal to the web plane. Similar to the experiment, a rigid body part, having larger thickness and higher yield stress, is attached to the loading edge to prevent the local yielding at the loading point. In the FE model, the rotation about y and z directions of the points located at the lines connecting the flanges and web were considered to be free. Typical FE mesh division used in the modeling is shown in Fig. 3. In which, a finer mesh division is adopted near the fixed end where the local buckling and concentration of plastic deformation may take place. This mesh contains 728 elements and has a total of 4698 degrees of freedom. The stress-strain curve is described by the power rule which may be written as follows.

$$\sigma = \sigma_y ( 1 + b \varepsilon_p )^N \qquad (1)$$

In which the constant $b$ and $N$ can be determined from the material constants, i.e. yield stress ($\sigma_y$), maximum tensile stress ($\sigma_T$) and elongation ($\varepsilon_T$). The values of these constants for the material used in the comparison are given in Table 1. Further, for the multi surface plasticity model employed in this study, the stress-strain curve is divided into five segments with five constant tangent modulus.

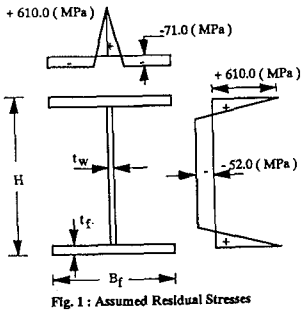


Fig. 1 : Assumed Residual Stresses

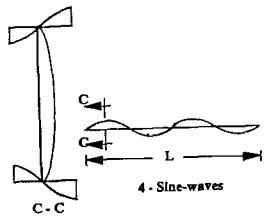


Fig. 2 : Assumed initial deflections

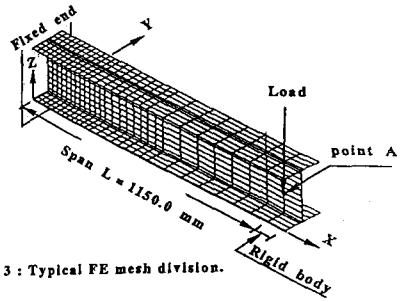


Fig. 3 : Typical FE mesh division.

Table 1 : Dimensions of the Models used in the Comparison with Experiment

| Specimen | $B_f$ (mm) | $t_f$ (mm) | H (mm) | $t_w$ (mm) | L (mm) | $\sigma_y$ (Mpa) | $\sigma_T$ (Mpa) | $\varepsilon_T$ % | YR % | Constants in the power rule b | N |
|---|---|---|---|---|---|---|---|---|---|---|---|
| A | 160 | 10 | 250 | 7.5 | 1150 | 610 | 681 | 9.2 | 89.8 | 61.323 | .1043 |
| B | 160 | 6.4 | 242.8 | 4.6 | 1150 | 610 | 681 | 9.2 | 89.8 | 61.323 | .1043 |

Where

$B_f$, $t_f$, H and $t_w$ are as shown in Fig. 1

YR = Yield-to-tensile strength ratio

$\sigma_y$ = Yield stress

$\sigma_T$ = Maximum tensile strength

$\varepsilon_T$ % = Elongation

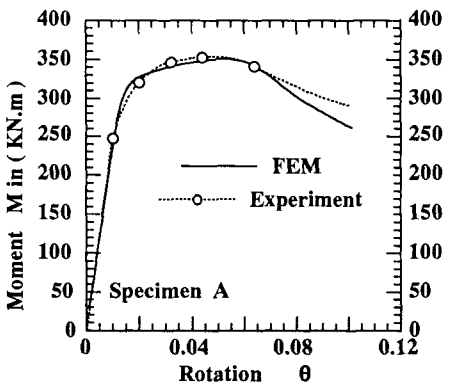


Fig. 4 : Moment-rotation diagram for specimen A

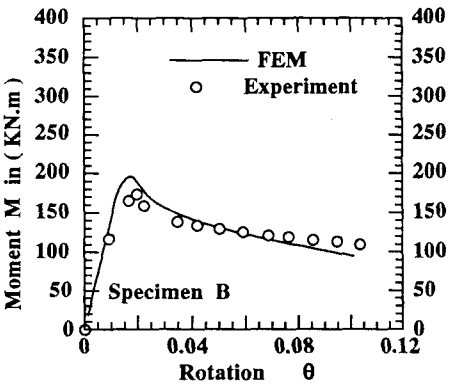


Fig. 5 : Moment-rotation diagram for specimen B

Figures 4 and 5 compare the moment-rotation curves of the numerical results with the experimental ones. The rotation, $\theta$, is defined as the deflection at the loading point divided by the distance from the loading point to the fixed end.

A good agreement is observed between the predicted and experimental ultimate moment and the corresponding rotation for the specimen A. However, the predicted ultimate moment was about 12% higher than the experimental one for the specimen B. This could be attributed to the sensitiveness of this specimen to the initial imperfection. The sensitiveness of this specimen comes from the fact that the flange width-to-thickness and web height-to-thickness ratios are relatively large. Also, a slight differences in the post ultimate behavior was found in both specimens. This may be because of, in the analyses, the rotation of loading edge about the longitudinal axis (x-axis) was assumed to be free during the entire loading path. From the comparison shown in the above, it can be concluded that the present method of numerical simulation is considered to be

effective to analyzing the behavior of I-section cantilever beam.

## 3. Investigated Models and Parameters

The investigated models in this study were divided into two groups (*G* and *M*) according to the examined parameters. The models in group *G* were considered to study the effect of geometrical parameters and those in group *M* were considered to study the effect of strain hardening of the material. All the models have similar **F E** mesh, boundary conditions, loading condition and assumed initial deflection pattern to those used in the comparison with the experiments. However, the residual stresses were not considered in this parametric study. The geometrical parameters were represented by flange width-to-thickness parameter $\lambda_f$ and web height-to-thickness parameter $\lambda_w$. While the yield-to-tensile strength ratio was selected to investigate the effect of work-hardening properties in group *M*. All models have the same web height-to-flange width ratio and the beam length-to-web height ratio. **Table 2** lists the detailed data of models investigated in this study.

**Table 2 : Description of the Investigated Models and Parameters.**

| Group | Model | $\lambda_w$ | $\lambda_f$ | Loading Type | Mechanical Properties of the materials used | Remarks |
|---|---|---|---|---|---|---|
| G | G1 | 0.3 | 0.4 | Monotonically increasing load | See Fig. 7 | |
| | G2 | 0.3 | 0.6 | | | |
| | G3 | 0.3 | 0.8 | | | |
| | G4 | 0.3 | 1.0 | | | |
| | G5 | 0.4 | 0.4 | | | |
| | G6 | 0.4 | 0.6 | | | |
| | G7 | 0.4 | 0.8 | | | |
| | G8 | 0.4 | 1.0 | | | |
| | G9 | 0.5 | 0.4 | | | |
| | G10 | 0.5 | 0.6 | | | |
| | G11 | 0.5 | 0.8 | | | |
| | G12 | 0.5 | 1.0 | | | |
| | G1-C | 0.3 | 0.4 | Cyclic loading | See Fig. 7 | Combined isotoropic-kinematic hardening rule is considered |
| | G9-C | 0.5 | 0.4 | | | |
| | G4-C | 0.3 | 1.0 | | | |
| | G12-C | 0.5 | 1.0 | | | |
| M | M1-LYR | 0.3 | 0.4 | Monotonically increasing load | YR = 65 % | |
| | M1-HYR | 0.322 | 0.43 | | YR = 90 % | |
| | M4-LYR | 0.3 | 1.0 | | YR = 65 % | |
| | M4-HYR | 0.322 | 1.074 | | YR = 90 % | |
| | MC-LYR | 0.3 | 1.0 | Cyclic loading | YR = 65 % | Full kinematic hardening rule is assumed |
| | MC-HYR | 0.322 | 1.074 | | YR = 90 % | |

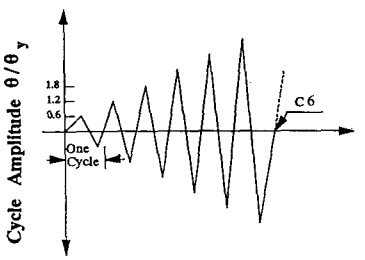


**Fig. 6 : Cyclic Loading Sequence**

Where

$$\lambda_f = \frac{B_f}{2\,t_f}\sqrt{\frac{12(1-\nu^2)}{\pi^2 k_f}\frac{\sigma_y}{E}} \qquad \text{and} \qquad \lambda_w = \frac{H-t_f}{t_w}\sqrt{\frac{12(1-\nu^2)}{\pi^2 k_w}\frac{\sigma_y}{E}}$$

**In which**

**$k_f$ and $k_w$ are the buckling coefficients of the flange and web, respectively**
**( $k_f$ = 0.425 and $k_w$ = 23.9 ) [11)]**

**$\nu$ = Poisson's ratio = 0.3**

**$\sigma_y$ = yield stress**

**E = Young's Modulus**

**$B_f$, $t_f$, H and $t_w$ are as shown in Fig. 1**

Two typical loadings were considered in this work, namely, monotonically increasing load and cyclic loading with continuously increasing amplitudes. The cyclic load was applied with displacement control, and a typical loading history is

shown in **Fig. 6**. The hysteretic loops were generated by increasing the vertical deflection at the cantilever end incrementally. For the first cycle, the vertical deflection, δ, was imposed at the cantilever end in the downward direction to a value of 0.6 times the yield deflection $\delta_y$. When this peak value was reached, the deflection was reduced incrementally to zero, returning to its initial position. Deflection was then imposed in the opposite direction, i.e. upwards until the peak value of -0.6 $\delta_y$. After this, it was incrementally decreased again until zero deflection, thus completing the first cycle. The cycles were repeated with increasing each peak deflection for subsequent cycles by 0.6 times $\delta_y$ until a total of thirteen cycles were completed.

## 4. Computed Results and Discussion

The behavior of I-section cantilever beam under monotonically increasing loads are represented by the normalized moment-rotation diagrams. Further, the phenomena is examined with respect to both normalized ultimate moment $M_u / M_y$ and maximum rotation $\theta_{max}/\theta_y$. Where $M_y$, $\theta_y$, $M_u$ and $\theta_{max}$ are defined as the initial yield moment, the corresponding yield rotation, the ultimate moment capacity and the corresponding maximum rotation capacity, respectively. While the behavior under cyclic loadings is represented by the hysteretic loops. In addition, the effect of cyclic loading is examined through the comparison between the envelop and monotonic curves, as well as the accumulated absorbed energies. The absorbed energy is described as the average energy absorbed per unit volume. In other words, its normalized value with respect to $M_y \theta_y$ is referred to as normalized absorbed energy which corresponds to the area under the normalized moment-rotation diagram, i.e.

$$\hat{E} = \int M \, d\theta / M_y \theta_y \qquad (2)$$

### 4.1 Effect of Geometrical Parameters

Sixteen models, belonging to group G were employed to investigate the effect of geometrical parameters $\lambda_f$ and $\lambda_w$ on the behavior of built-up I-section cantilever beam. The values of $\lambda_f$ and $\lambda_w$ were chosen to cover the practical design range in constructing I-beam. Twelve models were subjected to monotonically increasing loads and other four models were subjected to cyclic loadings with continuously increasing amplitude. All models belonging to this group have web height-to-flange width ratio (H/B) of 250/160 and length-to-web height ratio (L/H) of 1150/250. The non-linear combined isotoropic-kinematic hardening model with same material properties reported by Petersson and Popov [5] was adopted in this group. **Figures 7-(a) and (b)** show the virgin and saturated curves as well as the weighting function $W$ of this material, respectively.

#### 4.1.1 Computed Results under monotonically increasing load

Normalized moment-rotation diagrams for different values of $\lambda_f$ in case of $\lambda_w = 0.3$ is shown in **Fig. 8**. In these cases, the beams reach the first yield moment followed by the inelastic local buckling of the flange near the fixed end where the plastic hinge is formed. The local buckling in the bottom flange facilitates the local buckling in the web to develop a failure mechanism. Then, the beams reach their ultimate moments. Shown in **Fig. 9** is the normalized ultimate moment $M_u / M_y$ versus $\lambda_w$ for four different values of $\lambda_f$. From these results, it is found that the ultimate moment is reduced with an increase in $\lambda_f$ and this reduction increases with $\lambda_w$. This is attributed to the fact that the normalized ultimate moment has a strong relation with the normalized buckling load of each component plates which is inversely proportional to $\lambda_f$ or $\lambda_w^2$ [12].

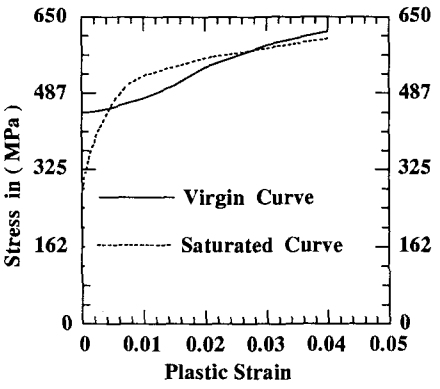


a) Virgin and saturated stress-strain curve

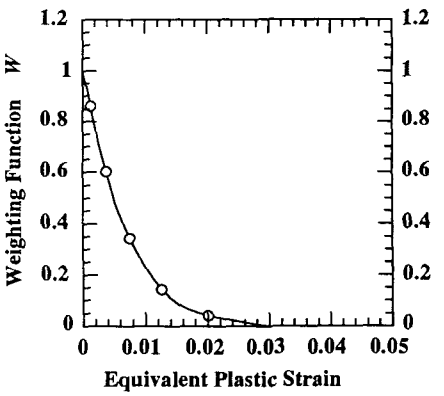


b) Weighting function, W

Fig. 7 : Properties of the material used in group G

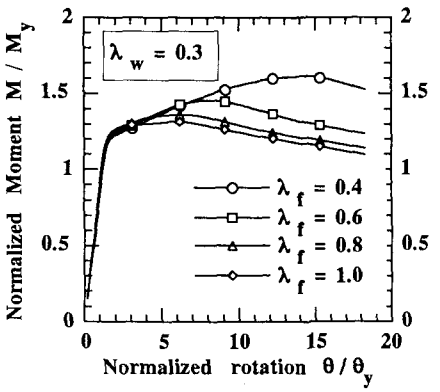


Fig. 8 : Normalized moment-rotation diagrams for different Values of $\lambda_f$ in case of $\lambda_w = 0.3$

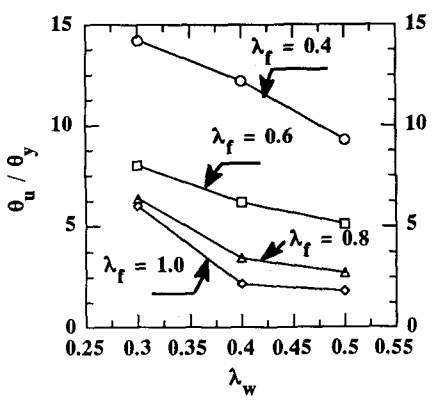


Fig. 9 : Normalized ultimate moment versus $\lambda_w$ for different values of $\lambda_f$

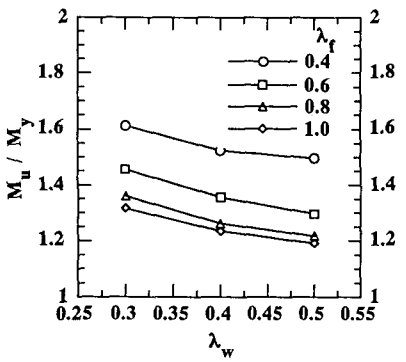


Fig. 10 : Normalized maximum rotation versus $\lambda_w$ for different values of $\lambda_f$

Same tendency can be observed on the deformation capacity as shown in **Fig. 10**, in which the normalized maximum rotation versus $\lambda_w$ for different values of $\lambda_f$ are plotted.

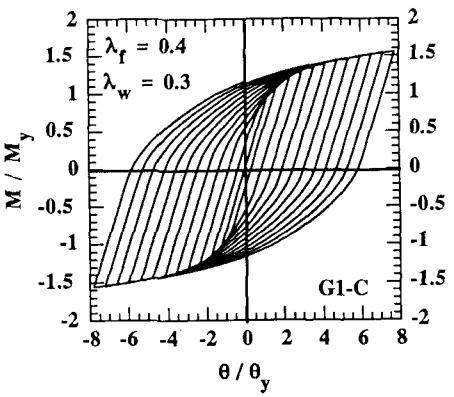


Fig. 11-(a)

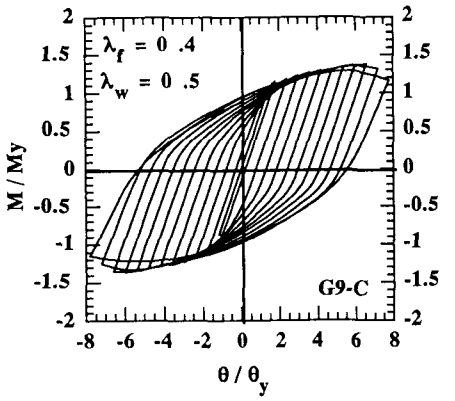


Fig. 11-(b)

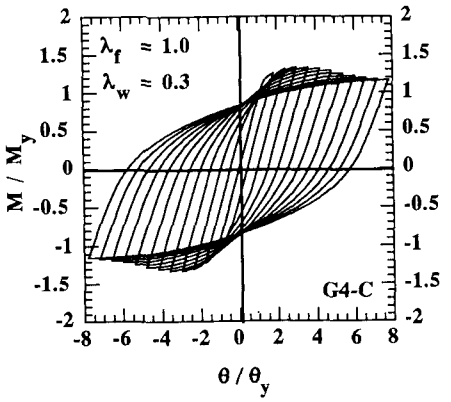


Fig. 11-(c)

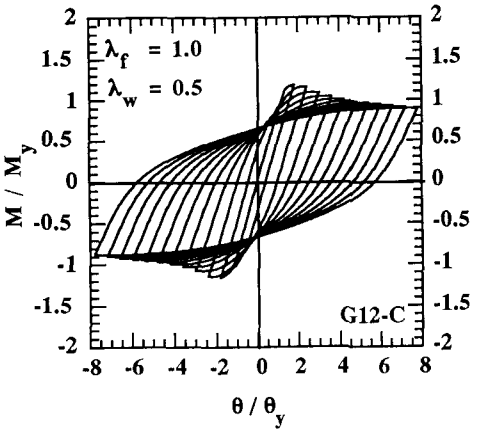


Fig. 11-(d)

**Figs. 11 : Normalized moment-rotation hysteretic loops**

### 4.1.2 Computed Results under cyclic loading

Normalized moment $M/M_y$ versus rotation $\theta/\theta y$ hysteretic loops for models G1-C, G9-C, G4-C and G12-C are shown in **Figs. 11-(a), (b), (c)** and **(d)**, respectively. It can be seen that, The behavior of model G1-C $(\lambda_f = 0.4\ ,\ \lambda_w = 0.3)$ is very stable because no local buckling occurred in the flanges nor web. However, in the case G9-C $(\lambda_f = 0.4\ ,\ \lambda_w = 0.5)$, the degradation of the strength and the member stiffness are found to be stable up to a later stage of loading sequence, they then rapidly decreased due to the instability in the web, as it will be seen from the final deformed shape. Comparison between the computed results of G1-C $(\lambda_f = 0.4\ ,\ \lambda_w = 0.3)$, G4-C $(\lambda_f = 1.0\ ,\ \lambda_w = 0.3)$ and G12-C $(\lambda_f = 1.0\ ,\ \lambda_w = 0.5)$ shows that an increase in $\lambda_f$ has a significant effect on increasing the deterioration of maximum strength and member stiffness and the rate of this deterioration increases with $\lambda_w$. This is attributed to the cyclic growth of local buckling developed in the top and the bottom flanges as well as the web. Same tendency are found on the cumulative absorbed energy as shown in **Fig.12**. In which, the largest value of cumulative absorbed energy is found in case G1-C $(\lambda_f = 0.4\ ,\ \lambda_w = 0.3)$, while the smallest value is found in case G12-C $(\lambda_f = 1.0\ ,\ \lambda_w = 0.5)$.

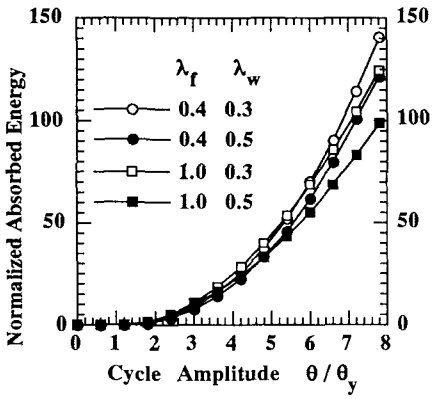


**Fig. 12 : Normalized cumulative absorbed energy**

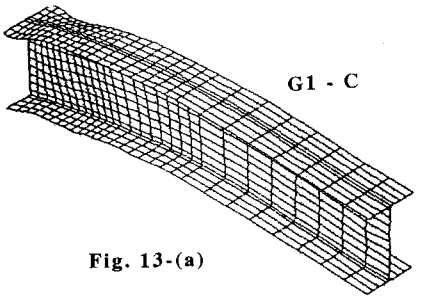


**Fig. 13-(a)**

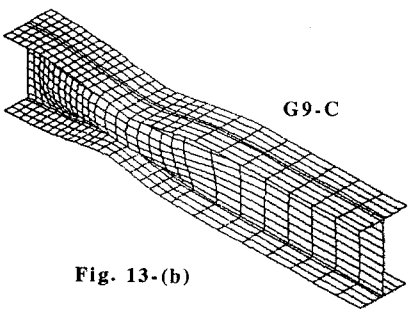


**Fig. 13-(b)**

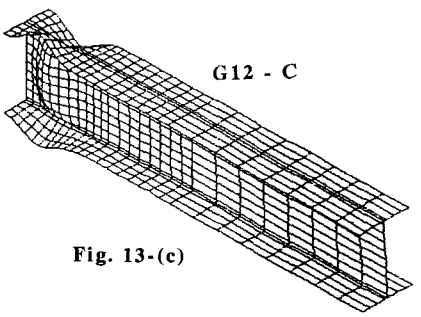


**Fig. 13-(c)**

**Figs. 13 : Final deformed shape**

To examine the effect of geometrical parameters on the failure modes, the final deformed shapes at the end of the loading sequence for three extreme cases, namely, G1-C, G9-C and G12- *C* are shown in **Figs 13-(a), (b)** and **(c)**, respectively. While, the distribution of the deflection along the free edge of the flange and the mid height of the web are shown in **Figs. 14-(a), (b), (c), (d), (e)** and **(f)**, respectively. As these figures show, almost no local buckling occurred in the case G1-C. However, in the case G9-C, the failure mode is due to the instability of the web, in one-wave along the beam length, causing the both flanges on the top and bottom to deform into the web direction. While, in the case G12-C, the failure mode is due to the local buckling of the flanges in the opposite directions causing the web near the fixed end to buckle locally .

To show the effect of geometrical parameters on the plastic strain concentration, the distribution of total equivalent plastic strain at top and bottom surfaces over free edge of the flange for G1-C and G12-C are plotted in **Figs. 15-(a)** and **(b)**, respectively. Two peaks are observed. One at the end is due to the stress concentration caused by the constrained from the fixed end. The other is caused by the local buckling. In case of G1-C, which shows small local buckling, the maximum value of the total equivalent plastic strain is found at the fixed end. Thus the crack may be initiated at the fixed end. While, in case of G12-C, with large local buckling, the crack may also initiate from the locally buckled part.

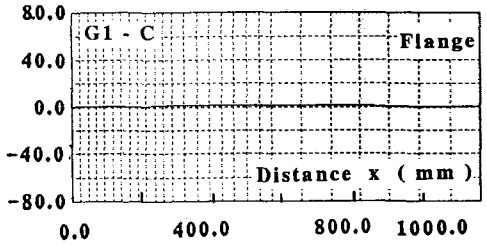


Fig. 14-(a)

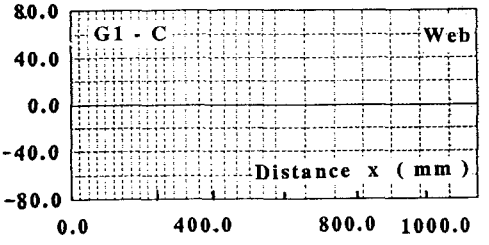


Fig. 14-(b)

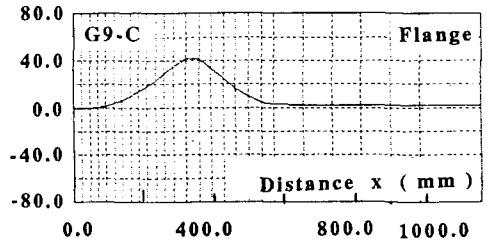


Fig. 14-(c)

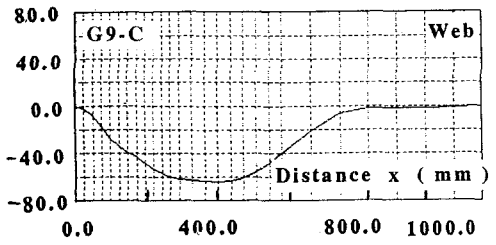


Fig. 14-(d)

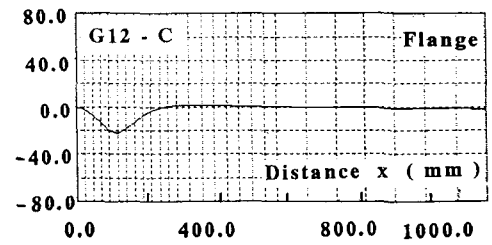


Fig. 14-(e)

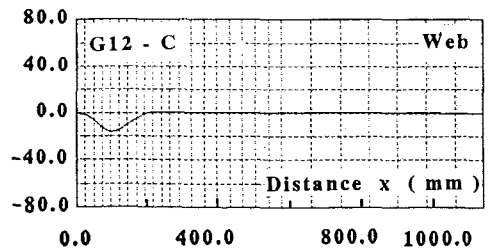


Fig. 14-(f)

Figs. 14 : Local buckling size in the end of loading sequence

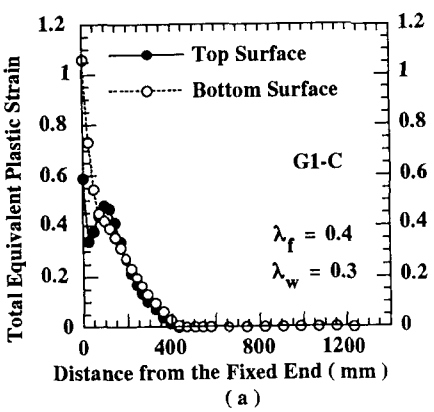


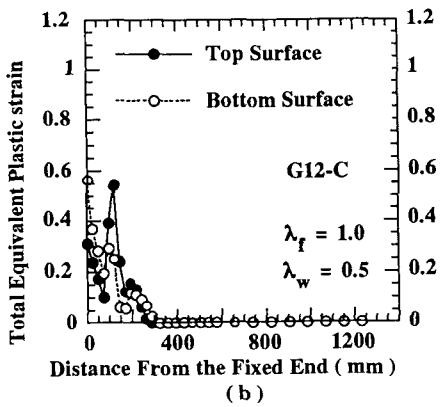


Figs. 15 : Distribution of total equivalent plastic strain along the free edge of the bottom flange

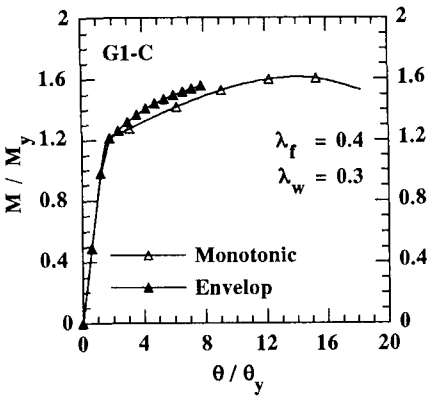


Fig. 16-(a)

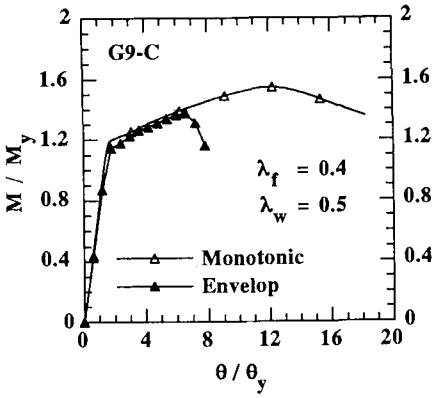


Fig. 16-(b)

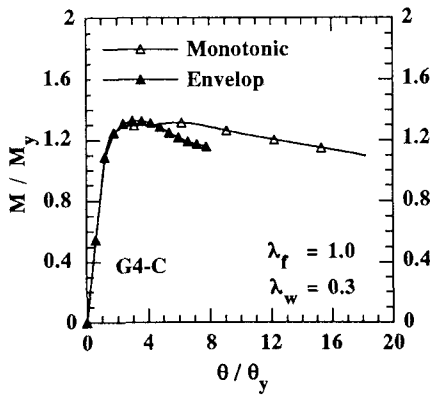


Fig. 16-(c)

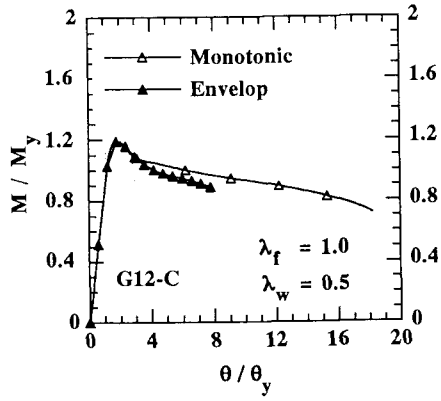


Fig. 16-(d)

Figs. 16 : Comparison between envelop and monotonic Curves

In addition, to demonstrate the difference between the results of cyclic loading and monotonically increasing load, a comparison between the envelop curve and monotonic curve for four different geometries are plotted in **Figs. 16-(a), (b), (c)** and **(d)**. It can be seen that, in the case G1-C, the envelop curve shows a slightly higher values of the strength compared to the monotonic curve. This is because the behavior of this model is not governed by the local buckling but mostly governed by cyclic properties of the material which follows non-linear combined isotoropic-kinematic hardening rule. The isotoropic hardening part is thought to be the reason of such higher values of the strength. In the case G12-C, almost no reduction in the maximum strength and the corresponding rotation capacity due to cyclic loading is observed. After the maximum strength is reached, the values of the envelop curve are slightly smaller than those of the monotonic curve. While in the cases G9-C and G4-C, the maximum strength and the corresponding maximum rotation capacity of the envelop curve are significantly smaller compared to those for the monotonic loading. This is due to the cyclic growth of local buckling (or plastic deformation) developed in the flanges and/or web during the cyclic loading. Thus, the monotonic curves can not always be used to predict the maximum strength and rotation capacity under cyclic loading.

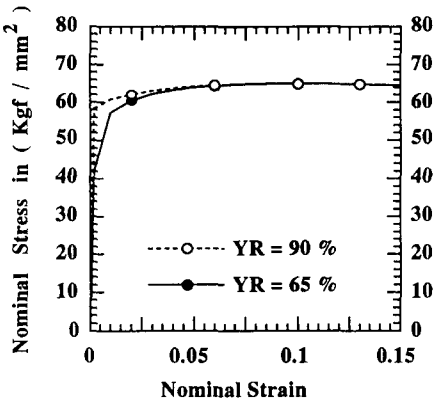


Fig. 17 : Nominal stress-strain curve

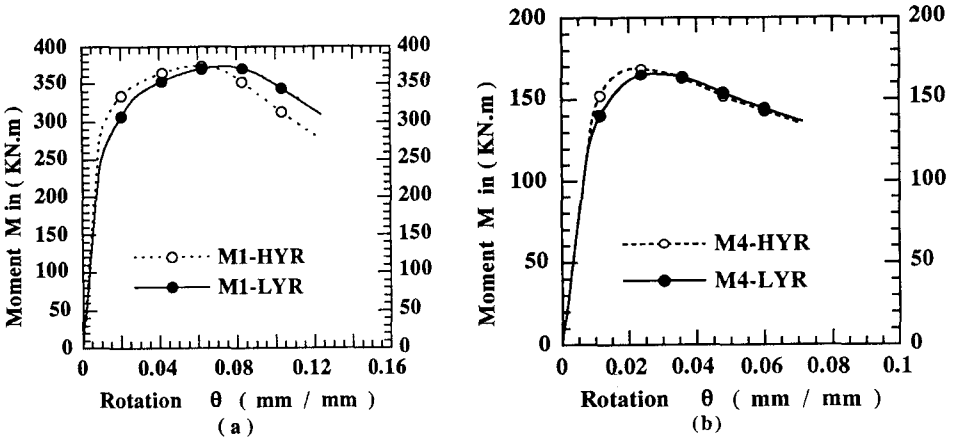


Figs. 18 : Effect of YR on the moment-rotation diagrams

### 4.2 Effect of work-hardening of the material

To investigate the effect of work-hardening of the material on the performance of I-beam, two typical materials are considered. The nominal stress-strain curves of these materials are shown in **Fig. 17**. The yield -to- tensile stress ratios (*Y R*) are 65% and 90%, while both the elongation and the maximum tensile strength are assumed to be constant ($\varepsilon_T$ = 10% and $\sigma_T$ = 65 kgf/mm$^2$). It is clear that the tangent modulus in the strain hardening region is larger when the material has lower *Y R*. The power rule is used to describe the stress strain curve.

Although, serial computations are performed to clarify the effect of **YR** on the behavior of I-beam with different geometries, only the results of two typical geometries are reported here, due to the limited space in this paper. For each geometry, the dimensions of the beam are kept constant for both low and high **YR** materials. Since the yield stress of **LYR** material is smaller than that of **HYR** material, the slenderness parameters are smaller than those of **HYR** material as shown in Table 2. It was assumed that the material follows the pure kinematic hardening rule of Mroz model. The detailed

description of the investigated models are given in Table 2 (group $M$). The effect of **Y R** on the behavior of I-beam is examined under monotonically increasing loads as well as cyclic loading with increasing displacement amplitude.

**Figures 18-(a)** and **(b)** show the effect of **Y R** on the moment-rotation diagrams for the two different geometries, respectively. It can be noticed that, when the flanges and the web are relatively thick, the ultimate moment of case M1-LYR is almost equal to that of case M1-HYR. While, when the the flanges are relatively thin, the ultimate moment of case M4-LYR is slightly smaller compared to that of case M4-HYR. However, an increase in the maximum rotation capacity, by 5.0%, and 23.0%, is observed for both geometries, respectively, when the material has lower **Y R**. This may be attributed to the fact that the tangent modulus in the strain hardening region is larger when the material has lower **Y R** and it delays the occurrence of local buckling in the component plates. Consequently, the beam can show more deformation capability when the ultimate moment is reached. Another reason may be related to the smaller values of slenderness parameters in cases M1-LYR and M4-LYR compared to those in cases M1-HYR and M4-HYR, respectively.

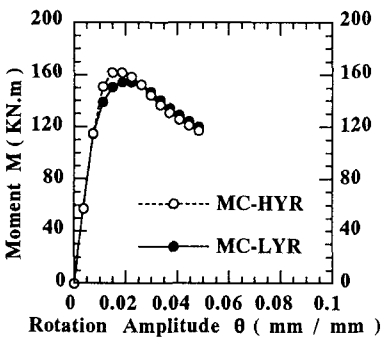


Fig. 19 : Effect of YR on the Cyclic Response ( Envelop Curves)

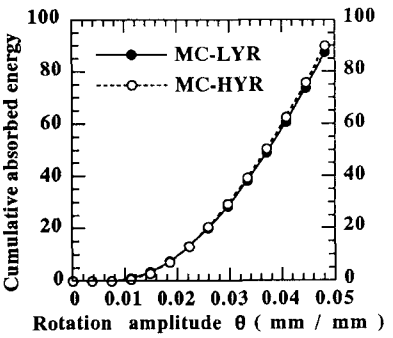


Fig. 20 : Effect of YR on the cumulative absorbed energy

To examine the effect of **Y R** of the material on the behavior of I-beam under cyclic loading, two cases are considered, namely, MC-LYR and MC-HYR as shown in Table 2. These two cases were subjected to cyclic loading with continuously increasing displacement amplitude as described above in Fig. 6. The yield stress of low **Y R** material is used to normalized the displacement amplitude by initial yield displacement $\delta_y$ for both cases.

The cyclic response represented by envelop curves is illustrated in **Fig. 19**. Further, the cumulative absorbed energy versus the rotation amplitude for the two cases is shown in **Fig. 20**. It can be noticed that, the maximum rotation capacity which corresponds to the maximum moment is larger in case of MC-LYR compared to that of MC-HYR. Although, the ultimate moment of MC-LYR is slightly decreased. Further, almost no difference between the cumulative absorbed energy of the two materials is observed, as shown in Fig. 20.

## 5. Conclusions

The behavior of built-up I-section cantilever beam under both the application of cyclic loading as well as monotonically increasing load is investigated. The Finite Element Method (**FEM**) considering material and geometrical non-linearities was

employed in this research. The investigated factors were the slenderness ratios of the flanges and the web, the type of loading, and the yield-to-tensile strength ratio of the material. Based on the computed results, the following conclusions can be drawn.

1) The present method of numerical modeling is considered to be effective to analyzing the behavior of I-section cantilever beam.
2) Local buckling in the flange and/or the web are greatly influenced by the slenderness parameter of each component plates. This local buckling becomes a major cause of the reduction in strength and rotation capacity under monotonically increasing load. Further, the deterioration of strength and absorbed energy due to local buckling becomes more appreciable when the cyclic load is applied. Such a possibility can be prevented by selecting a smaller slenderness parameter $\lambda$ of the flange and the web.
3) Utilizing material having lower yield-to-tensile strength ratio (**Y R**) improves the maximum rotation capacity. Although, it slightly decreases the ultimate strength. While, the total absorbed energy of the beam is not sensitive to the **Y R** of the material when the material exhibits pure kinematic hardening.

Further research is needed to study the effect of the other work-hardening properties of the material such as, the elongation, the length of the yield plateau and the cyclic hardening of the material. Also, experimental studies would be necessary to confirm the computational results reported here.

## REFERENCES


1) Fukumoto, Y. and Lee, G. C., ( Eds. ) : Stability and ductility of steel structures under cyclic loading, Proc. of US-Japan Joint Seminar, Osaka, Japan, July 1-3, 1991.
2) Mindlin, R.D., J. Appl. Mech., vol. 18, pp. 31, 1951.
3) Hughes, T. J. R., Taylor, R. L., and Kanoknukulchai, w., : A simple and efficient Finite Element for plate bending, Int. J. Num. Meth. Engng, vol. 11, pp. 1529-1543, 1977
4) Hughes,T. J. R., Cohen, M., and Haroun, M., : Reduced and selective integration techniques in the Finite Element analysis of plates, J. of Nucl. Eng. Des., vol. 46, pp. 203-222, 1978
5) Petersson, H., and Popov, E.P., : Constitutive relations for generalized loadings, J. of Eng. Mech. Division, ASCE, vol. 103, pp. 611-627, 1977.
6) Popov, E.P., and Petersson H., : Cyclic metal plasticity : experiments and theory, J. of Eng. Mech.Division, ASCE, vol. 104, pp. 1371-1388, 1978.
7) Mosaddad, B., and Powell, G.H., : Computational models for cyclic plasticity, rate dependance, and creep in finite element analysis, Report No. UCB/EERC-82/26, University of California at Berkeley, CA, 1982.
8) Crisfield, M. A., : A fast incremental iterative solution procedure that handles ' snap-through',Comp. & Stru., vol. 13, pp. 55-62, 1981
9) Crisfield, M. A., : Non-linear Finite Element analysis of solids and structures,John wiley & Sons,1991
10) Takahashi, F.,: Improvement of loading carrying capacity of structure members by using modified H-section beam, M.Sc. Thesis, Osaka Univ., Faculty of Eng., Welding and Production Eng. Dept., 1993. ( in Japanees )
11) Column Research Committee of Japan, ( Eds. ) : Handbook of structural stability, Japan, 1971.
12) Li, S., and Reid, S. R., : The plastic buckling of axially compressed square tubes, ASME J. of Appl. Mech., vol. 59, pp. 276-282,1992


(Received on 16 September, 1993)